Journal of the Brazilian Society of Mechanical Sciences and Engineering (2022) 44:362
https://doi.org/10.1007/s40430-022-03659-9

REVIEW

A finite element model for a bi-layered piezoelectric plate-strip with initial stresses under a time-harmonic force

Ahmet Daşdemir[1]

Received: 23 August 2021 / Accepted: 27 June 2022 / Published online: 25 July 2022

Abstract

The novelty of this study is presenting the analytical approach to investigate the dynamic response and the forced vibration by a time-harmonic force of a bi-layered piezoelectric plate-strip with initial stresses, resting on a rigid foundation. Material properties are varied perpendicular to the free surface of the plate-strip according to a simple power-law distribution. Firstly, the nonlinear mechanical equations of motion are linearized within the scope of the three-dimensional linearized theory of elastic waves in initially stressed bodies (TLTEWISB). Furthermore, using the piezoelectricity material properties, linear electrical governing equations are derived. Next, the problem under consideration is solved by the finite element method (FEM) to determine, especially the frequency response of the body. The approach is verified by the previous results in the literature. In numerical results, the influences of the initial stress, the height ratio of the layers, thickness ratio, and dimensionless frequency parameters on the dynamic response and the forced vibration of the bi-layered piezoelectric plate-strip are presented and discussed in detail.

Keywords Forced vibration · Frequency response · Initial stress · Piezoelectric material · Time-harmonic force

1 Introduction

Piezoelectricity is the appearance of electric potential or a voltage in the structures when subject to mechanical stress. Nowadays, piezoelectric materials are of great interest from research communities on smart materials and structures that play key roles in some desirable directions for various engineering devices such as nano-sensors, nano-actuators, and nano-resonators. Therefore, the mechanical problems related to the piezoelectric structures are under the great attention of many researchers around the world. The theoretical background of the piezoelectric materials and their mechanical properties were given by Yang [30].

Due to certain factors, dynamic vibration problems exhibit nonlinear wave propagation. This makes it difficult to analyze relevant mechanical researches. Therefore, to properly approximate the nonlinear distributions and dynamic behaviors in the system under consideration, quite several theoretical approaches were developed. While beginning the twentieth century, the first serious attempts (i.e., so-called Three Dimensional Linearized Equations (TDLE)) were introduced by Southwell [29] and Biezeno and Henky [8] to be able to examine the mentioned nonlinear wave propagation problems. The development process of this theory dating back to the present day has significantly been contributed by many scientists such as Trefftz [34], Biot [9], Neuber [23], and Green et al. [15]. Due to different needs over time, the TDLE has been updated by some researchers such as Guz [16], Zubov [39], Tiersten [32], Ogden [24], Akbarov and Guz [2], and Reddy [26]. In this study, the three-dimensional linearized theory of elastic waves in initially stressed bodies (TLTEWISB) that were developed by Guz [17] and is one of the most popular theories of recent days will be considered. This theory allows researchers the opportunity to more easily examine the nonlinear wave distribution case caused by the initial stress state in the

Technical Editor: Aurelio Araujo.

✉ Ahmet Daşdemir
ahmetdasdemir37@gmail.com

[1] Department of Mathematics, Faculty of Arts and Sciences, Kastamonu University, 37150 Kastamonu, Turkey

problem under consideration. Some detailed information about the TLTEWISB is presented by Akbarov [6].

In the framework of the TLTEWISB, many mechanical problems have been studied by a great number of scientists. The influence of the initial stress on the forced vibration caused by the dynamic loading of a rectangular plate with a cylindrical hole around the hole was analyzed by Yeşil [31]. The dynamic problem on the dispersion of Lamb waves in a triple-layered elastic plate with initial stresses was investigated by Zamanov and Agasiyev [37]. The finite element model of a plate-strip with initial stress subjected to an inclined time-harmonic force was developed by Eröz [13]. The dynamic problem for shear-spring-type imperfect contact conditions in the pre-stressed bi-layered elastic system with finite lengths was considered by Akbarov et al. [4]. The axisymmetric wave propagation in a pipe subjected to lateral surface pressure based on a first-power hypo-elastic constitutive model was studied by Wen-tao et al. [36]. The dispersion relations of the flexural waves in the bi-layered hollow cylinder with imperfect contact between layers were derived by İpek [19]. The influence of the initial stress state on the Lamb wave propagation in the composite system with an elastic core bonded to the piezoelectric faces was investigated by Kurt et al. [22]. Using the finite element method, a dynamical stress field problem in a pre-stressed sandwich plate-strip with elastic layers and a piezoelectric core through imperfect contact conditions in both normal and tangential directions was approximately solved by Daşdemir [10]. Based on the linearized Navier–Stokes equations for inviscid compressible fluids, the natural vibrations of the inhomogeneously pre-stressed multi-layered hollow sphere including the compressible barotropic inviscid fluid were analyzed by Seydimaliyev et al. [28].

The miscellaneous ability of piezoelectric bodies to transform mechanical energy into electrical energy and vice versa has led to the need to examine many problems of various configurations since their suitable for varieties of applications including sensors and actuators. This requirement impresses the theory according to which the problem will be handled, the assumptions under which the problem will be solved, which solution method will be applied, and many other issues. For this purpose, in the current literature, there exist many papers devoted to investigating the mechanical behavior of multi-layered piezoelectric materials today.

The reflection and refraction of quasi-longitudinal waves across an interface between two pre-stressed anisotropic piezoelectric media with different properties were investigated by Abd-alla and Alsheikh [3]. The Lamb problem related to the system consisting of a piezo-electric covering layer resting on a piezoelectric half-plane for the case wherein both half-planes are polled in the perpendicular direction to the horizontal surface was numerically solved by Akbarov and İlhan [5] applying the exponential Fourier transformation. Note that the paper of Abd-alla and Alsheikh [3] was improved to eliminate some drawbacks by Guo and Wei [14]. Instead of most mechanical considerations in the current literature, many innovations, such as there are three initial stress states under the continuous conditions of all electrical and mechanical qualities for the arbitrary inclined polarization directions of quasi longitudinal and quasi traverse waves, were examined by Guo and Wei [14]. The paper by Akbarov and İlhan [5] was extended to the case where the system has different polarization configurations, e.g., the upper layer is polarized along the parallel direction of the interface while the lower one along the vertical direction of the interface, by İlhan and Koç [20]. The total electro-mechanical potential energy and energy release rate (ERR) caused by the uniformly distributed normal forces acting on the two parallel open cracks in a pre-stressed plate-strip made of an elastic core and adjacent piezoelectric faces were explored by Akbarov and Yahnioğlu [7]. The spectral element method (SEM) was used to analyze the free vibration of a smart functionally graded (FG) plate sandwiched with two piezoelectric layers within the scope of the first-order shear deformation theory by Abad and Rouzegar [1]. A variable kinematics plate modeling based on the Sublaminate Generalized Unified Formulation (SGUF) for composite plates with bonded piezoelectric plies working in extension mode was developed by D'Ottavio et al. [12]. The reflection and transmission of wave propagation through a piezoelectric semiconductor slab sandwiched by two piezoelectric half-planes were studied by Jiaoa et al. [21]. The influences of initial stress on the propagation of Lamb and SH waves in multilayer piezoelectric composites using the Legendre polynomial method were reported by Othmani et al. [25]. The reflection and transmission of quasi-longitudinal plane (QP) waves in two piezoelectric semiconductor half-planes with two types of initial stresses, i.e., normal stress and shear stress, were studied by Sahu et al. [27].

The mathematical approach for investigating a forced vibration problem in a pre-stressed piezoelectric plate-strip resting on a rigid foundation was recommended by Daşdemir [11]. In this paper, the dynamical electro-elastic problem in the bi-layered piezoelectric plate-strip, subjected to a time-harmonic force, with initial stresses standing on a rigid ground is considered. In the plane strain–stress state, the mechanical and electrical governing equations are derived within the fundamental principle of the three-dimensional linearized theory of electro-elastic waves in initially stressed bodies (TLTEEWISB). Based on the variational formulation and the virtual work principle, the finite element model (FEM) for the problem under the suggestion is developed. Furthermore, some numerical results illustrating the various problem parameters such as initial stress or dimensionless frequency parameter of the dynamic external loading are presented. It should be noted that, throughout the paper, the conventional summation rule is applied over the repeated indices.

2 Problem formulation

Consider a piezoelectric system of a dual plate-strip standing on a rigid ground. According to the scheme in Fig. 1, the layers are of the uniform length $2L$ and the heights h_1 and h_2, and the total

height of the body to h. The superscripts "(1)" and "(2)" are used to specify the top and bottom layers, respectively.

Each material is to be assumed linear, homogeneous, and isotropic and is polled in the vertical direction to the free surface. The geometrical relations can be represented by fourth- and third-order tensors of the material parameters. But, we can utilize Voigt's reduction notation to reduce the mentioned representations to second-order tensors, namely, $pq \to i$ and $rs \to j$, where $i, j = 1, 2$. In this case, we can give the second-order geometrical relations, in the matrix form, as follows:

$$\begin{pmatrix} \sigma_{11}^{(m)} \\ \sigma_{22}^{(m)} \\ \sigma_{12}^{(m)} \\ D_1^{(m)} \\ D_2^{(m)} \end{pmatrix} = \begin{pmatrix} c_{11}^{(m)} & c_{13}^{(m)} & 0 & 0 & e_{31}^{(m)} \\ c_{13}^{(m)} & c_{33}^{(m)} & 0 & 0 & e_{33}^{(m)} \\ 0 & 0 & c_{44}^{(m)} & e_{15}^{(m)} & 0 \\ 0 & 0 & e_{15}^{(m)} & \gamma_{11}^{(m)} & 0 \\ e_{31}^{(m)} & e_{33}^{(m)} & 0 & 0 & \gamma_{33}^{(m)} \end{pmatrix} \begin{pmatrix} \varepsilon_{11}^{(m)} \\ \varepsilon_{22}^{(m)} \\ 2\varepsilon_{12}^{(m)} \\ E_1^{(m)} \\ E_2^{(m)} \end{pmatrix}, \tag{1}$$

where $\sigma_{ij}^{(m)}$, $D_i^{(m)}$, $\varepsilon_{ij}^{(m)}$, and $E_i^{(m)}$ are the corresponding components of the stress, electric displacement, strain, and electric field vectors, respectively. Moreover, $c_{ij}^{(m)}$, $e_{ij}^{(m)}$, and $\gamma_{ij}^{(m)}$ in the coefficient matrix are the mechanical, the piezoelectric, and the dielectric material parameters.

A static (tension or compression) force is applied to each layer along the edge sides before sticking together. For the initial state of the corresponding parameters, an additional upper index "0" will also be used. Following, a time-harmonic force is applied to the midpoint of the top surface of the system being put on the ground. Note that the origin of the coordinate system is located at this point. In the initial state, the position of the points in the Cartesian system of coordinates x_i can be determined by the Lagrangian coordinates x_i'. As a result, a pre-stressed dynamic-stress-field problem occurs. For the current investigation, the following assumptions are taken into account:

(i) the initial stress-state is exactly homogeneous and static;
(ii) the magnitudes of the dynamic deformations are considerably smaller than the initial state's ones; and
(iii) there is a rigidly clamped state between the layers.

Based on the above assumptions, the current investigation can be conducted according to the TLTEEWISB. In this case, the initial stress state in the system can be described as follows:

$$\sigma_{11}^{(m),0} = q^{(m)}, \quad \text{and} \quad \sigma_{ij}^{(m),0} = 0 \quad \text{for} \quad ij \neq 11, \tag{2}$$

where $q^{(m)}$ is a constant value of the initial stress value for the mth layer. Besides, according to the piezoelectric effects of the materials, the following initial electric displacements also occur:

$$D_1^{(m),0} = d^{(m)} \quad \text{and} \quad D_2^{(m),0} = 0, \tag{3}$$

where $d^{(m)}$ is a known constant. In 1880, Curie brothers experimentally discovered that electric charges in the piezoelectric materials are linearly proportional to the mechanical loading. Hence, using the constitutive equations yields the interrelationship

$$d^{(m)} = \frac{c_{13}^{(m)} e_{33}^{(m)} - c_{33}^{(m)} e_{31}^{(m)}}{\left(c_{13}^{(m)}\right)^2 - c_{11}^{(m)} c_{33}^{(m)}} q^{(m)}$$

between the initial mechanical stress and the initial electric displacement.

According to the foregoing explanations and the fundamental principles of the TDLE, the nonlinear mechanical and electromechanical equations of motion are

$$\frac{\partial}{\partial x_i'}\left[\sigma_{ik}^{(m)}\left(\delta_{kj} + \frac{\partial u_j^{(m)}}{\partial x_k'}\right)\right] = \rho \frac{\partial^2 u_i^{(m)}}{\partial t^2} \tag{4}$$

and

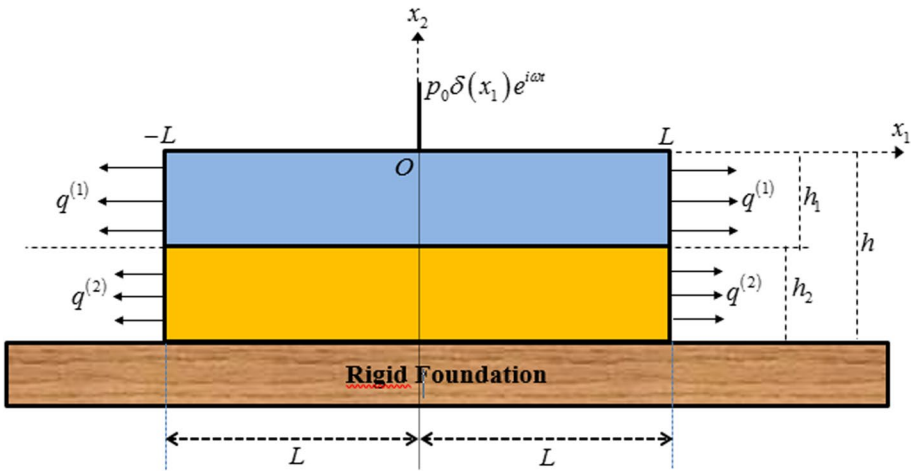

Fig. 1 The geometry of the problem

$$\frac{\partial}{\partial x_i'}\left[D_n^{(m)}\left(\delta_{in}+\frac{\partial u_i^{(m)}}{\partial x_n'}\right)\right]=0, \tag{5}$$

where $u_i^{(m)}$ is the corresponding mechanical displacement component and δ_{ij} is the Kronecker delta. Note that since the dynamic force varies harmonically with the time parameter t, all the problem fields can be purified as $[\cdot]^{(m)}=[\hat{\cdot}]^{(m)}e^{i\omega t}$, where i is the complex unit and e is Euler's famous constant. For simplicity, the hats will be neglected after this. Moreover, Eqs. (4) and (5) hold for the initial perturbation state, namely

$$\frac{\partial}{\partial x_i'}\left[\sigma_{ik}^{(m),0}\left(\delta_{kj}+\frac{\partial u_j^{(m),0}}{\partial x_k'}\right)\right]=0, \tag{6}$$

and

$$\frac{\partial}{\partial x_i'}\left[D_n^{(m),0}\left(\delta_{in}+\frac{\partial u_i^{(m),0}}{\partial x_n'}\right)\right]=0. \tag{7}$$

Considering the perturbations $\sigma_{ik}^{(m)}=\tilde{\sigma}_{ik}^{(m)}+\tilde{\sigma}_{ik}^{(m),0}$, $D_i^{(m)}\cong\tilde{D}_i^{(m)}+\tilde{D}_i^{(m),0}$, and $u_j^{(m)}\cong\tilde{u}_j^{(m)}+\tilde{u}_j^{(m),0}$, the elasto-electro-dynamic equations take shape

$$\frac{\partial}{\partial x_i'}\left[\left(\tilde{\sigma}_{ik}^{(m)}+\tilde{\sigma}_{ik}^{(m),0}\right)\left(\delta_{kj}+\frac{\partial\left(\tilde{u}_j^{(m)}+\tilde{u}_j^{(m),0}\right)}{\partial x_k'}\right)\right]+\rho^{(m)}\omega^2\tilde{u}_i^{(m)}=0 \tag{8}$$

and

$$\frac{\partial}{\partial x_i'}\left[\left(\tilde{D}_n^{(m)}+\tilde{D}_n^{(m),0}\right)\left(\delta_{in}+\frac{\partial}{\partial x_n'}\left(\tilde{u}_i^{(m)}+\tilde{u}_i^{(m),0}\right)\right)\right]=0, \tag{9}$$

where $\rho^{(m)}$ is the mass density of the mth layer. According to our three assumptions, the linear equilibrium equations are written as

$$\frac{\partial}{\partial x_k'}\tilde{\sigma}_{ij}^{(m),0}=0 \quad \text{and} \quad \frac{\partial}{\partial x_i'}\tilde{D}_n^{(m),0}=0 \tag{10}$$

As a result, Eqs. (8) and (9) can be reorganized as

$$\begin{aligned}&\frac{\partial}{\partial x_i'}\Bigg[\tilde{\sigma}_{ik}^{(m),0}+\underline{\tilde{\sigma}_{ik}^{(m),0}\frac{\partial\tilde{u}_j^{(m),0}}{\partial x_k'}}+\tilde{\sigma}_{ik}^{(m),0}\frac{\partial\tilde{u}_j^{(m)}}{\partial x_k'}\\&+\tilde{\sigma}_{ik}^{(m)}+\underline{\tilde{\sigma}_{ik}^{(m)}\frac{\partial\tilde{u}_j^{(m)}}{\partial x_k'}}+\underline{\tilde{\sigma}_{ik}^{(m)}\frac{\partial\tilde{u}_j^{(m),0}}{\partial x_k'}}\Bigg]\\&+\rho^{(m)}\omega^2\tilde{u}_i^{(m)}=0.\end{aligned} \tag{11}$$

and

$$\begin{aligned}&\frac{\partial}{\partial x_i'}\Bigg[\tilde{D}_i^{(m),0}+\underline{\tilde{D}_n^{(m),0}\frac{\partial\tilde{u}_i^{(m),0}}{\partial x_n'}}+\tilde{D}_n^{(m),0}\frac{\partial\tilde{u}_i^{(m)}}{\partial x_n'}\\&+\tilde{D}_i^{(m)}+\underline{\tilde{D}_n^{(m)}\frac{\partial\tilde{u}_i^{(m)}}{\partial x_n'}}+\underline{\tilde{D}_n^{(m)}\frac{\partial\tilde{u}_i^{(m),0}}{\partial x_n'}}\Bigg]=0,\end{aligned} \tag{12}$$

respectively.

Here, the underlined terms in the above equations can be neglected. Since $\tilde{\sigma}_{ik}^{(m),0}$ and $\tilde{D}_i^{(m),0}$ are of a constant value and ignoring the upper tilde over the quantities with the coordinate transformation procedure $\tilde{x}_i=x_i/h$, the following linear elasto-electro-dynamic equations are obtained:

$$\sigma_{ij,j}^{(m)}+\sigma_{11}^{(m),0}u_{i,11}^{(m)}+\rho^{(m)}\omega^2h^2u_i^{(m)}=0, \tag{13}$$

$$D_{i,i}^{(m)}+D_1^{(m),0}u_{i,i1}^{(m)}=0. \tag{14}$$

Besides, the following boundary-contact conditions are valid:

$$\sigma_{12}^{(1)}\Big|_{x_2=0}=0, \quad \sigma_{22}^{(1)}\Big|_{x_2=0}=-p_o\delta\left(x_1\right), \tag{15}$$

$$\left(q^{(m)}u_{j,1}^{(m)}+\sigma_{1j}^{(m)}\right)\Big|_{x_1=\mp L/h}=0, \quad \left(D_1^{(m)}+d^{(m)}u_{1,1}^{(m)}\right)\Big|_{x_1=\mp L/h}=0, \tag{16}$$

$$u_i^{(1)}\Big|_{x_2=-h_1/h}=u_i^{(2)}\Big|_{x_2=-h_1/h}, \quad \sigma_{12}^{(1)}\Big|_{x_2=-h_1/h}=\sigma_{12}^{(2)}\Big|_{x_2=-h_1/h}c, \tag{17}$$

$$u_i^{(2)}\Big|_{x_2=-1}=0, \quad \varphi^{(1)}\Big|_{x_2=0}=0, \quad and, \quad \varphi^{(2)}\Big|_{x_2=-1}=0, \tag{18}$$

where $\delta(.)$ is the Dirac-delta function and φ is the electrical potential. Note that there are geometrical relations $\varepsilon_{ij}^{(m)}=\left(u_{i,j}^{(m)}+u_{j,i}^{(m)}\right)/2$ and $E_i^{(m)}=-\varphi_{,i}^{(m)}$. Here, the subscripts after the commas imply spatial coordinate differentiation.

The physical meanings of the boundary conditions may be summed up as follows: Eq. (15) is mechanical traction-free conditions due to the external time-harmonic force; further, Eq. (16) is mechanically and electrically open conditions at the edges of the plate-strip. While Eq. (17) is complete clamped conditions between the layers, Eq. (18) is mechanically free and electrically open (short-circuit) conditions caused by the interruption of mechanical and electrical wave propagation by the rigid foundation.

3 Solution methodology

For an approximate solution, it is preferable to employ the usual finite element method (FEM) based on the virtual work principle [38]. For this purpose, consider the mechanical test functions $w_i^{(m)}$ and the electrical test function $\phi^{(m)}$. It must be noted that the equations of motion and the related boundary-contact conditions hold for these functions.

Using Gauss' famous theorem following the integration over the problem domain by summing after the multiplication of Eqs. (13) and (14) with test functions $w_i^{(m)}$ and $\phi^{(m)}$, respectively, yields

$$\int_D \left[P_{ij}^{(m)} w_{i,j}^{(m)} - \rho^{(m)}\omega^2 h^2 u_i^{(m)} w_i^{(m)} + R_i^{(m)} \phi_{,i}^{(m)}\right] dD - \int_S \left[P_{ij}^{(m)} w_i^{(m)} n_j + R_i^{(m)} n_i \phi^{(m)}\right] dS = 0, \tag{19}$$

where D is the problem domain, S is the boundary of the plate-strip, and n_i is the unit outward vector. In the above equation, the following notations are used:

$$P_{ij}^{(m)} = \sigma_{ij}^{(m)} + \sigma_{kj}^{(m),0} u_{i,k}^{(m)} = p_{ijkn}^{(m)} u_{n,k}^{(m)} + r_{ijk}^{(m)} \varphi_{,k}^{(m)} \tag{20}$$

and

$$R_i^{(m)} = D_i^{(m)} + D_i^{(m),0} u_{j,i}^{(m)} = r_{ijk}^{(m)} u_{j,k}^{(m)} - s_{ik}^{(m)} \varphi_{,k}^{(m)}, \tag{21}$$

where

$$\begin{aligned}
&p_{1111}^{(m)} = c_{11}^{(m)} + q_{11}^{(m)}, p_{1122}^{(m)} = c_{13}^{(m)},\\
&p_{1212}^{(m)} = c_{44}^{(m)}, p_{1221}^{(m)} = c_{44}^{(m)} + q_{11}^{(m)},\\
&p_{2112}^{(m)} = c_{44}^{(m)}, p_{2121}^{(m)} = c_{44}^{(m)},\\
&p_{2211}^{(m)} = c_{13}^{(m)}, p_{2222}^{(m)} = c_{33}^{(m)},\\
&r_{111}^{(m)} = d^{(m)}, r_{112}^{(m)} = e_{15}^{(m)},\\
&r_{121}^{(m)} = e_{15}^{(m)} + d^{(m)}, r_{211}^{(m)} = e_{31}^{(m)},\\
&r_{222}^{(m)} = e_{33}^{(m)}, s_{11}^{(m)} = \gamma_{11}^{(m)},\\
&s_{22}^{(m)} = \gamma_{33}^{(m)}.
\end{aligned} \tag{22}$$

Applying the boundary-contact conditions in (15)-(18) to Eq. (19) yields

$$\int_D \left[P_{ij}^{(m)} w_{i,j}^{(m)} - \rho^{(m)}\omega^2 h^2 u_i^{(m)} w_i^{(m)} + R_i^{(m)} \phi_{,i}^{(m)}\right] dD + \int_{-L/h}^{L/h} p_o \delta(x_1) w_2^{(1)}\Big|_{x_2=0} dx_1 = 0 \tag{23}$$

or in another form,

$$\int_D \left[\sigma_{ij}^{(m)} \varepsilon_{ij}^{(m),w} + \theta_{ij}^{(m),u} w_{i,j}^{(m)} + D_i^{(m)} \phi_{,i}^{(m)} + \theta_{ij}^{(m),s} \phi_{,i}^{(m)} - \rho^{(m)}\omega^2 h^2 u_i^{(m)} w_i^{(m)}\right] dD + \int_{-L/h}^{L/h} p_o \delta(x_1) w_2^{(1)}\Big|_{x_2=0} dx_1 = 0, \tag{24}$$

where $\varepsilon_{ij}^w = \left(w_{i,j} + w_{j,i}\right)/2$, $\theta_{ij}^u = \sigma_{kj}^0 u_{i,k}$, and $\theta_{ij}^s = D_i^0 u_{j,i}$. Equations (23) and (24) are the weak form of the problem under consideration.

Following, changing the functions $w_i^{(m)}$ and $\phi^{(m)}$ with the related displacement functions $\delta u_i^{(m)}$ and electric potential $\delta\varphi^{(m)}$ that satisfy the equations of motion and the corresponding boundary-contact conditions to obtain the variational formulation of the problem, the following operations can be done:

$$\begin{aligned}
0 &= \int_D \left[\sigma_{ij}^{(m)} \delta\varepsilon_{ij}^{(m)} + \theta_{ij}^{(m),u} \delta u_{i,j}^{(m)} + D_i^{(m)} \delta\varphi_{,i}^{(m)} + \theta_{ij}^{(m),s} \delta\varphi_{,i}^{(m)} - \rho^{(m)}\omega^2 h^2 u_i^{(m)} \delta u_i^{(m)}\right] dD + \int_{-L/h}^{L/h} p_o \delta(x_1) \delta u_2^{(1)}\Big|_{x_2=0} dx_1\\
&= \int_D \left[\left(\sigma_{ij}^{(m)} + r_{kij}^{(m)}\right)\delta\varepsilon_{ij}^{(m)} + \sigma_{kj}^{(m),0} u_{i,k}^{(m)} \delta u_{i,j}^{(m)} + \left(r_{kij}^{(m)} u_{i,j}^{(m)} - s_{kn}^{(m)} \varphi_{,n}^{(m)}\right)\delta\varphi_{,k}^{(m)} - \rho^{(m)}\omega^2 h^2 u_i^{(m)} \delta u_i^{(m)}\right] dD\\
&\quad + \int_{-L/h}^{L/h} p_o \delta(x_1) \delta u_2^{(1)}\Big|_{x_2=0} dx_1\\
&= \int_D \left[\left(\sigma_{ij}^{(m)} + \sigma_{kj}^{(m),0} u_{i,k}^{(m)}\right)\delta u_{i,j}^{(m)} + r_{kij}^{(m)}\left(\varphi_{,k}^{(m)} \delta u_{i,j}^{(m)} + u_{i,j}^{(m)} \delta\varphi_{,k}^{(m)}\right) - s_{kn}^{(m)} \varphi_{,n}^{(m)} \delta\varphi_{,k}^{(m)} - \rho^{(m)}\omega^2 h^2 u_i^{(m)} \delta u_i^{(m)}\right] dD\\
&\quad + \int_{-L/h}^{L/h} p_o \delta(x_1) \delta u_2^{(1)}\Big|_{x_2=0} dx_1\\
&= \int_D \left[p_{mjkl}^{(m)} u_{k,l}^{(m)} \delta u_{i,j}^{(m)} + r_{kij}^{(m)}\left(\varphi_{,k}^{(m)} \delta u_{i,j}^{(m)} + u_{i,j}^{(m)} \delta\varphi_{,k}^{(m)}\right) - s_{kn}^{(m)} \varphi_{,n}^{(m)} \delta\varphi_{,k}^{(m)} - \rho^{(m)}\omega^2 h^2 u_i^{(m)} \delta u_i^{(m)}\right] dD\\
&\quad + \int_{-L/h}^{L/h} p_o \delta(x_1) \delta u_2^{(1)}\Big|_{x_2=0} dx_1\\
&= \delta\left[\int_D \left[\frac{1}{2} p_{ijkl}^{(m)} u_{k,l}^{(m)} u_{i,j}^{(m)} + r_{kij}^{(m)} \varphi_{,k}^{(m)} u_{i,j}^{(m)} - \frac{1}{2} s_{kn}^{(m)} \varphi_{,n}^{(m)} \varphi_{,k}^{(m)}\right] dD - \frac{1}{2}\int_D \rho^{(m)}\omega^2 h^2 \left(u_i^{(m)}\right)^2 dD + \int_{-L/h}^{L/h} p_o \delta(x_1) \delta u_2^{(1)}\Big|_{x_2=0} dx_1\right],
\end{aligned} \tag{25}$$

where $\underline{\sigma}_{ij}$ is the mechanical part of the respective stress component. Let us introduce the notations

$$\mathrm{P} = \frac{1}{2}\int_D \left[p_{ijkl}^{(m)} u_{k,l}^{(m)} u_{i,j}^{(m)} + 2r_{kij}^{(m)} \varphi_{,k}^{(m)} u_{i,j}^{(m)} - s_{kn}^{(m)} \varphi_{,n}^{(m)} \varphi_{,k}^{(m)}\right] dD,$$

$$\mathrm{K} = \frac{1}{2}\int_D \rho^{(m)} h^2 \left(u_i^{(m)}\right)^2 dD, \quad \textit{and}$$

$$\mathrm{Z} = -\int_{-L/h}^{L/h} p_o \delta(x_1)\delta u_2^{(1)}\Big|_{x_2=0} dx_1,$$

where P, K, and Z are the potential, kinetic, and virtual force energies, respectively. Hence, based on Hamilton's principle, the solution to our target problem is reduced to the form as follows:

$$\delta\left(\mathrm{P} - \omega^2 \mathrm{K} - \mathrm{Z}\right) = 0. \tag{26}$$

Based on the virtual work principle, the usual finite element method is used for numerical discussions. Let $B_m \subset B$ be master finite elements that satisfy $B_m \subset B$, $B_h = \bigcup_m B^{em}$, and $B_m \cap B_n = \emptyset$ for $m \neq n$. In this case, we investigate a generalized solution of the total energy functional in Eq. (26) for the displacements $\mathbf{u}_m = \left[u_{1m}\ u_{2m}\right] \in B_{um}$, the electrical fields $\mathbf{E}_m = \left[E_{1m}\ E_{2m}\right] \in B_{Em}$, and their virtual structures $\delta\mathbf{u}_m$ and $\delta\mathbf{E}_m$ in the form

$$\mathbf{u}_m \approx \mathbf{N}_{um}\tilde{\mathbf{u}}, \mathbf{E}_m \approx \mathbf{N}_{Em}\tilde{\mathbf{e}}, \delta\mathbf{u}_m \approx \mathbf{N}_{um}\delta\tilde{\mathbf{u}}, \quad \textit{and} \quad \delta\mathbf{E}_m \approx \mathbf{N}_{Em}\delta\tilde{\mathbf{e}}, \tag{27}$$

where $\tilde{\mathbf{u}}$ and $\tilde{\mathbf{e}}$ are the global vectors related to the nodal displacements and the nodal electrical fields, respectively, $\mathbf{N}_{um}$ is the matrix of the shape functions for the displacements, and $\mathbf{N}_{Em}$ is the row vector of the shape function for the electrical fields. In this paper, the eight-node smooth finite elements will be used, but this preference can be changed according to some requirements. Some invariants of the shape functions are presented by Hutton [18]. In this case, the nodal degrees of freedom (NDOF) can be organized, in a vector form, as follows:

$$u_m = \left[u_{m1}\ u_{m2}\right]^T = \left[u_{11}\ u_{12}\ \ldots\ u_{18}\ |\ u_{21}\ u_{22}\ \ldots\ u_{28}\right]^T$$

and

$$E_m = \left[E_{m1}\ E_{m2}\right]^T = \left[E_{11}\ E_{12}\ \ldots\ E_{18}\ |\ E_{21}\ E_{22}\ \ldots\ E_{28}\right]^T.$$

On the substitution of Eq. (27) into the total energy functional (26) and according to the general application principle of the FEM technique with very extensive operations and manipulations, the following matrix system of equations is obtained:

$$\left\{\mathbf{K}_{uu} - \omega^2 \mathbf{M}_{uu}\right\}\tilde{\mathbf{U}} + \mathbf{K}_{uE}\tilde{\mathbf{E}} = \mathbf{F}_u, \tag{28}$$

$$\mathbf{K}_{uE}\tilde{\mathbf{U}} + \mathbf{K}_{EE}\tilde{\mathbf{E}} = \mathbf{F}_E, \tag{29}$$

where $\mathbf{K}_{uu}$, $\mathbf{K}_{uE}$, and $\mathbf{K}_{EE}$ are the mechanical, electro-elastic, and electrical global stiffness matrices, respectively, and $\mathbf{M}_{uu}$ are the global mass matrix. Moreover, $\mathbf{F}_u$ and $\mathbf{F}_E$ are the mechanical and electrical global force vectors, respectively. It should be noted that, while the vector $\mathbf{F}_E$ is null, $\mathbf{F}_u$ has only a unique nonzero component according to the boundary-contact conditions. As a result, the matrix equations in Eqs. (28) and (29) can be amalgamated as follows:

$$\left(\mathbf{K} - \omega^2 \mathbf{M}\right)\mathbf{U} = \mathbf{F}, \tag{30}$$

where

$$\mathbf{K} = \begin{bmatrix} \mathbf{K}_{uu} & \mathbf{K}_{uE} \\ \mathbf{K}_{uE} & \mathbf{K}_{EE} \end{bmatrix}, \mathbf{M} = \begin{bmatrix} \mathbf{M}_{u_1} & 0 \\ 0 & \mathbf{M}_{u_2} \end{bmatrix},$$
$$\mathbf{U} = \begin{Bmatrix} \tilde{\mathbf{U}} \\ \tilde{\mathbf{E}} \end{Bmatrix}, \quad \text{and} \quad \mathbf{F} = \begin{Bmatrix} \mathbf{F}_u \\ \mathbf{F}_E \end{Bmatrix}. \tag{31}$$

It should be noted that due to the variational formulation in Eq. (26), the global matrices $\mathbf{K}$ and $\mathbf{M}$ are symmetric, real, and positive definite. This means that the matrix system in Eq. (30) is solvable and has a unique solution. Thus, the solution of this system gives the related displacement values and thus, according to Hooke's law, the required stress values can be obtained, and the desired numerical investigations can be made.

4 Numerical examples and discussions

This section presents a numerical investigation of the dynamic behavior of wave propagation under different cases. For this purpose, the following representations are firstly introduced:

$$\Omega^{(m)} = \omega h\sqrt{\frac{\rho^{(m)}}{c_{44}^{(m)}}},\ \eta^{(m)} = \frac{q^{(m)}}{c_{44}^{(m)}},\ \kappa^{(m)} = \frac{d^{(m)}}{2c_{44}^{(m)}},\ h_* = \frac{h}{2L},\ \hbar = \frac{h_1}{h_2},\ \hbar_j = \frac{h_j}{2L}, \text{ and } c = \frac{c_{44}^{(1)}}{c_{44}^{(2)}}, \tag{32}$$

where $\Omega^{(m)}$ is the dimensionless frequency parameter, $\eta^{(m)}$ is the initial stress parameter, $\kappa^{(m)}$ is the initial electric displacement parameter, h_* is the thickness ratio, $\mathcal{H}$ is the layers' thickness ratio, $\hbar_j$ is the layer-to-thickness ratio for ith layer, and $\boldsymbol{c}$ is the effective modulus ratio. Throughout the paper, all the numerical results will be governed at the interface plane between the plate-strip and rigid ground under the case wherein $\Omega = \Omega^{(1)} = \Omega^{(2)}$, $\Omega = 0$, $\eta = \eta^{(1)} = \eta^{(2)}$, $\eta = 0$, $h_* = 0.2$, and $\mathcal{H} =$ except for specified otherwise. To consider concrete numerical results, Oxide Nanobelts-1 (NBS - 1) in the upper layer, with $c_{44}^{(1)} = 34.5$ GPa, $e_{15}^{(1)} = 7.7$ C/m^2, and $\gamma_{11}^{(1)} = 0.9$ nF/m and Barium Titanate ($BaTiO_3$) in the lower layer, with $c_{44}^{(2)} = 44$ GPa, $e_{15}^{(2)} = 11.4$ C/m^2, and $\gamma_{11}^{(2)} = 1.115$ nF/m are chosen, as investigated by Daşdemir [11].

For validation of the numerical results, the case wherein each layer material is chosen as $BaTiO_3$ is considered. Therefore, the geometrical sketch of the plate-strip is exactly becoming similar form considered by Daşdemir [11]. Our numerical values must, therefore, approach those of the mentioned author under the same assumptions as NDOF increases. This foresight is proved by the graphs given in Fig. 2. Note that the starred graph was received from the paper of Daşdemir [11, pp. 426, Fig. 4.d-2], which is considered for the case wherein NDOF is equal to 15,075 was taken into account. As a result, the PC algorithm constructed for the current paper was validated.

For more validation, in the absence of an initial stress state, we consider the case where the thickness and length of the plate-strip are extending to infinity against the fixed certain values of thickness of the upper layer, i.e., $L \to \infty$ and $h \to \infty$. In this case, the geometry of our problem under consideration will evolve into the study of the dynamic response of a system consisting of a covering piezoelectric strip resting on a piezoelectric half-plane, which is the well-known Lamb's problem in mechanical investigations. It should be noted that a problem similar to the mentioned situation was investigated by Akbarov and İlhan [5] before. Figure 3 displays the graphs of the distributions of the stress $\sigma_{22}h/p_0$ versus x_1/h at the interface between the layers for certain values of the ratio $\mathcal{H}$. It follows from the graphs in Fig. 3 that, as $\mathcal{H}$, the numerical results from our PC programs and algorithm converge to those of Akbarov and İlhan [5], further validating the present mathematical modeling. It should be kept in mind that, in the graphs of Fig. 3, the bottom layer material is PZT-5H while the upper's is PZT-5A. Here, the double starred line is taken from the paper of Akbarov and İlhan [5].

Uflyand [35] reported an analysis of a dynamic stress field problem corresponding to a plate with infinite length resting on a rigid foundation by using the Fourier integral transformation method. Our problem under consideration is reduced to elastic media one by taking $c_{11}^{(m)} = c_{33}^{(m)} = \lambda^{(m)} + 2\mu^{(m)}$, $c_{13}^{(m)} = \lambda^{(m)}$, and $c_{44}^{(m)} = \mu^{(m)}$, where $\lambda^{(m)}$ and $\mu^{(m)}$ are the Lamé constants. In particular, for the case where $E^{(1)}/E^{(2)} = 1$, $\nu^{(1)} = \nu^{(2)} = 0.33$, and $\rho^{(1)}/\rho^{(2)} = 1$, oscillations of the graphs of Fig. 4 must approach the ones of Uflyand [35] as the thickness ratio $h_* \to 0$. Here, $E^{(m)}$ is the Young modulus, $\nu^{(m)}$ is the Poisson's ratio, and the piezoelectric and dielectric constants of the layer materials were taken to be zero. Figure 4 approves that this is indeed the case. Note that the triple asterisk indicates the results given by Uflyand [35]. In addition, when $h_* \to 0$ and $\Omega \to 0$, the problem turns into the famous Boussinesq problem, which was solved by Timoshenko and Godier [33, p. 85] and therefore, the numerical values of the normal stress $\sigma_{22}h/p_0$ must converge the corresponding analytical solution. Figure 4 proves that this prediction is valid. As a result, the validity and reliability of the computer program used in the present investigation were also checked by the agreement of the numerical results with the foregoing mechanical considerations.

In Fig. 5, the variations of the normal stress $\sigma_{22}h/p_0$ and the shear stress $\sigma_{21}h/p_0$ along the Ox_1-axis for certain values of the initial stress (both compression and tension) parameter η are shown. It should be noted that the negative and positive signs of the initial stress parameter η denote initial compression and tension, respectively. It seems that the absolute values of the stress $\sigma_{22}h/p_0$ increase with η, but the ones of $\sigma_{21}h/p_0$ decrease. The common result from Fig. 5 is that the influence character of the initial compression force is the opposite of that of the initial tension force. However, it follows from the distributions of the graphs that there are some regions wherein the absolute values of the stress $\sigma_{21}h/p_0$ decrease as the values of initial stress parameter η increase, such as $-x_1^*/h < x_1/h < x_1^*/h$. Besides, the

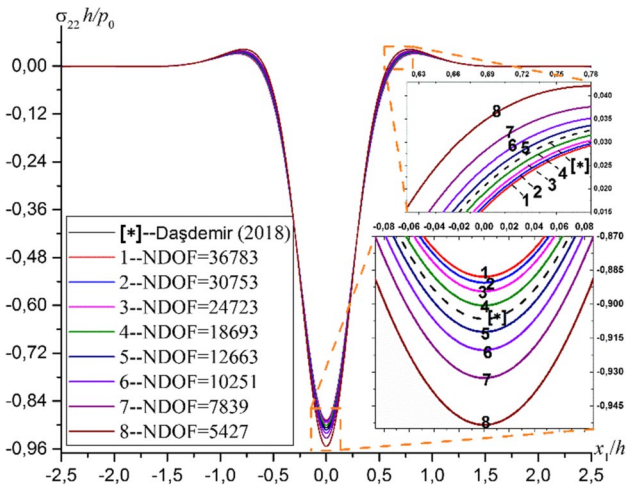

Fig. 2 Comparison of the numerical results for various values of NDOF with that of Daşdemir [11]

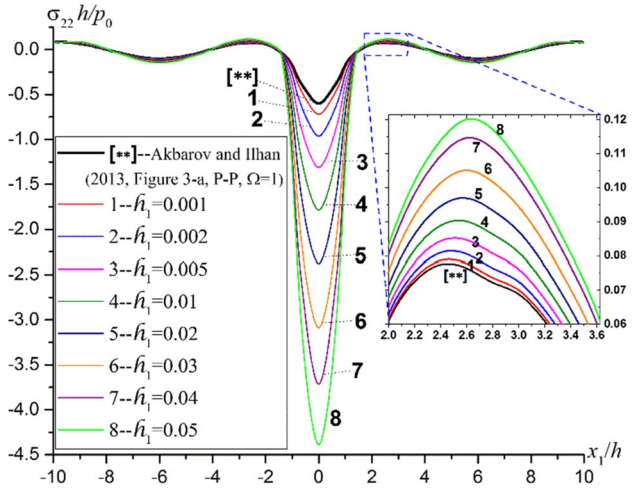

Fig. 3 Comparison of the results of the PC algorithm with the ones by Akbarov and İlhan [5]

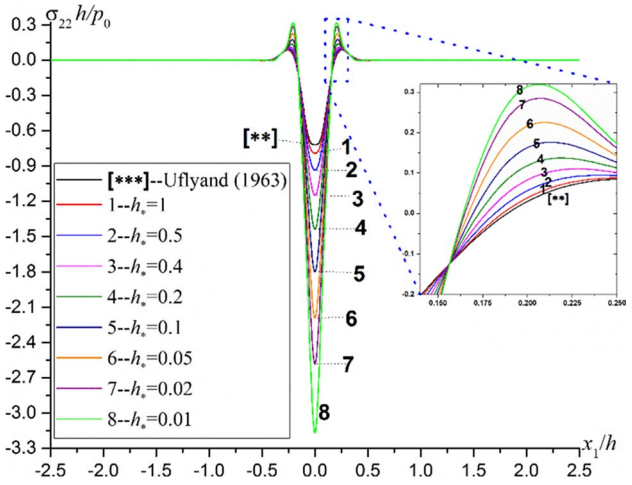

Fig .4 Cross-compare of the numerical results from the PC algorithm and the ones by Uflyand [35]

absolute values of $\sigma_{21}h/p_0$ decrease with the initial stress parameter η over the ranges $-x_1^{**}/h < x_1/h < -x_1^{*}/h$ and $x_1^{*}/h < x_1/h < x_1^{**}/h$. One can identify the values of x_1^{*}/h and x_1^{**}/h from Fig. 5b. In addition, the subsequent graphs of the stress $\sigma_{22}h/p_0$ versus the line x_1/h are more closely for two consecutive values of η, i.e., the initial stress parameter damps down the normal stress in the plate-strip. In particular, this damping is quite quick near the point $(0, -1)$.

Some general outcomes from the numerical findings in Figs. 2, 3, 4 and 5 may also be inferred. Besides, it follows that the Robin boundary conditions in Eq. (16) are validated by our numerical results since the values of the stresses converge to zero as $\eta \to 0$ at the side surfaces of the body. Since the dynamic force applied to the plate strip is perpendicular to the free surface, it is concluded that the distributions of the graphs are symmetric about the line $x_1/h = 0$ but the ones of the shear stress are anti-symmetric about that point, as expected. According to all the distributions, while $\sigma_{22}h/p_0$ reaches the unique absolute value at the point $x_1/h = 0$, $\sigma_{21}h/p_0$ attains two absolute values near the points $x_1/h = \mp 0.52$. These results agree well with the well-known mechanical considerations and confirm the proposed algorithm and PC programs once again.

To be able to consider the influence of certain problem parameters on the frequency response of the piezoelectric plate-strip, all the next numerical investigations will be conducted at the point $(0, -1)$.

In Fig. 6, the variations of $\sigma_{22}h/p_0$ versus the dimensionless frequency parameter Ω for various values of the initial stress parameter η are displayed. Further, graphs are also presented in the case wherein $h_* = 0.1$ (Fig. 6a), $h_* = 0.2$ (Fig. 6b), $h_* = 0.3$ (Fig. 6c), and $h_* = 0.4$ (Fig. 6d). The graphs prove that the absolute values of $\sigma_{22}h/p_0$ increase with Ω and the dependency between $\sigma_{22}h/p_0$ and Ω is non-monotonous. An increase in the value of the ratio h_* causes a decrease in the absolute values of $\sigma_{22}h/p_0$. The results coincide well with the preceding mechanical findings in the current literature. It seems that $\sigma_{22}h/p_0$ reaches a maximal value for certain values of Ω. These values are termed resonance values and are denoted by $\Omega *$. To be clear, the values of $\Omega *$ decrease as h_* increases. Further, the mentioned resonance values also increase with the initial stress parameter η. In particular, while the initial compression parameter exceeds the resonance mode of the stress $\sigma_{22}h/p_0$, the initial tension parameter blocks the mentioned mode. It is concluded from these numerical results that, increasing the initial tension applied to the layers reduces the stability of the system under consideration. On the contrary to this, the system becomes more stable as the initial compression increases. The initial stress parameter η has a great influence on the resonance mode of $\sigma_{22}h/p_0$. Note that the resonance values for each case can be observed from the graphs in Fig. 6. Furthermore, an increase in the values of h_* prevents the effect of the parameter η on the dispersion behavior of $\sigma_{22}h/p_0$. The influence the ratio h_* has on the frequency response of the plate-strip is not only quantitatively, but also qualitatively.

Figure 7 displays how the stress $\sigma_{22}h/p_0$ varies versus Ω for various values of the layers' thickness ratio $\hbar$. It is seen from the distributions of the graphs that the results presented above are identically valid here. For $\Omega < 1.2$, the absolute values of $\sigma_{22}h/p_0$ decrease as the ratio $\hbar$ increases. Besides, the resonance values also increase with the ratio $\hbar$. An increase in the values of the ratio $\hbar$ leads to damping the stress $\sigma_{22}h/p_0$. This means that the ratio $\hbar$ has a considerable effect on frequency response of the plate-strip, not only quantitatively, but also qualitatively. This result agrees well with our previous mechanical evaluations. Consequently,

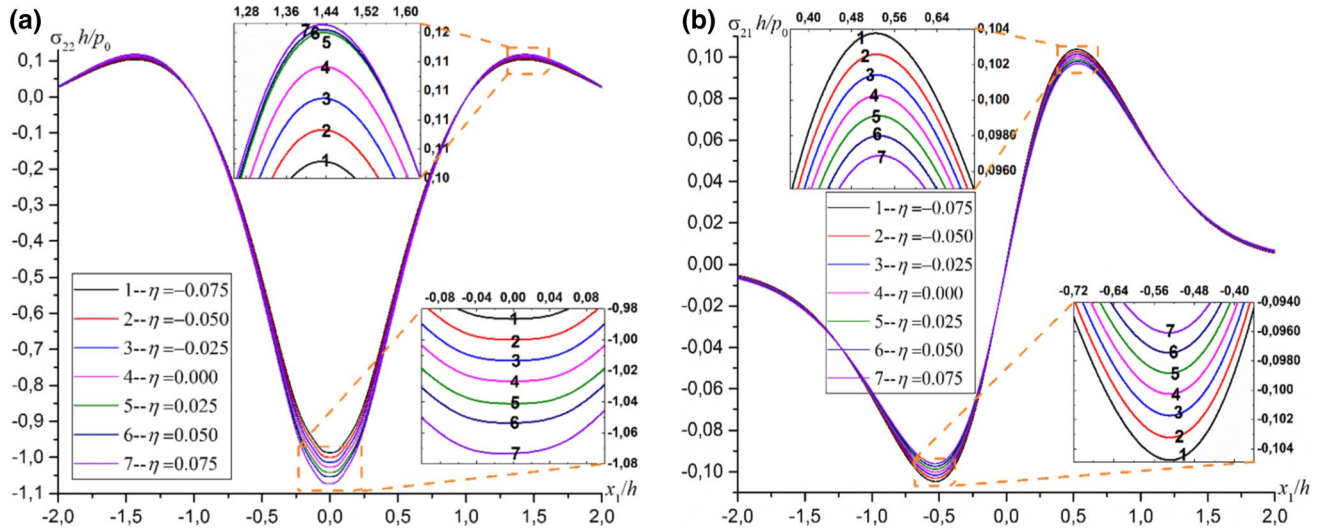

Fig. 5 Variations of **a** $\sigma_{22}h/p_0$ and **b** $\sigma_{21}h/p_0$ versus x_1/h for various values of η

we again validate the reliability and trustworthiness of our algorithm and implemented programs.

We now consider the influence of the effective modulus ratio $\boldsymbol{c}$ on the dynamic response of the bi-layered plate-strip. For this purpose, a case wherein each layer is selected as $BaTiO_3$ is taken into account but $c_{44}^{(1)}$ is changing manually while $c_{44}^{(2)}$ is fixed. As known, the mechanical material parameter $c_{44}^{(m)}$ is an elastic modulus for a piezoelectric medium; namely, it is a resistance to being deformed elastically of a body subjected to a force. The numerical results given in Fig. 8 allow observing the influence of the ratio $\boldsymbol{c}$ on the relationship between $\sigma_{22}h/p_0$ and Ω for the mentioned case. The graphs show that an increase in the values of the ratio $\boldsymbol{c}$ yields the absolute values of the normal stress $\sigma_{22}h/p_0$ to decrease. It is evident that the oscillating character of the distribution of the stress $\sigma_{22}h/p_0$ becomes more sensitive as the values of the ratio $\boldsymbol{c}$ decrease. This result appears since the effective modulus of the lower plate is greater than that of the upper plate. This agrees well with the previous mechanical findings, again proving the validity and the reliability of the PC algorithm. The resonance values $\Omega*$ of the stress $\sigma_{22}h/p_0$ decrease as the ratio $\boldsymbol{c}$ increases. This means that increasing the values of the ratio $\boldsymbol{c}$ prevents the resonance mode of the plate-strip. According to the graphs in Fig. 8, the numbers of the local extrema (maximums and minimums) of $\sigma_{22}h/p_0$ versus Ω decrease gradually with the ratio $\boldsymbol{c}$. As a result, the system under consideration becomes more stable as the values of $\boldsymbol{c}$ decrease. These results prove that the configuration of the body has a great role in the frequency response of the plate-strip. Hence, when investigating the frequency response of such a system, it is extremely important to identify the physical properties of the layers with high accuracy.

Figure 9 shows the dependency between $\sigma_{22}h/p_0$ and η for various values of the ratios h_* (Fig. 9a) and $\hbar$ (Fig. 9b). It can be said that the oscillations of the graphs depend linearly on the initial stress parameter (both the initial tension and compression) η. An increase in the values of h_* decreases the slopes of the graphs, namely, the influence of η on the dynamic response of $\sigma_{22}h/p_0$ decreases as h_* increases. A different situation exists for the ratio $\hbar$. To be clear, the influence of η on the stress distributions increases with the ratio $\hbar$. Besides, the effect of $\hbar h$ on the dependency between $\sigma_{22}h/p_0$ and η is bigger than that of h_*. The results from the graphs indicate that an increase in the thickness dimensions of the plate-strip reduces the influence of the initial stress parameter η on the stress $\sigma_{22}h/p_0$. Further, it can be said that both thickness ratios have a great role in the influence of η on the stress distributions. When the thickness of the upper layer is relatively greater than that of the bottom layer, the influence of the initial stress parameter η on the dynamic response of the normal stress $\sigma_{22}h/p_0$ is also greater. Note that while plotting the graphs, the thickness of the upper layer is constant.

5 Conclusions

In this paper, we insured a mathematical overview for a bi-layered piezoelectric plate-strip with initial stresses resting on a rigid foundation, subjected to a time-harmonic force. On the basis of the three-dimensional linearized theory of electro-elastic waves in initially stressed bodies (TLTEE-WISB), the equations of motion were developed and the resultant forced vibration problem was solved using the finite element model (FEM). The following are some of the conclusions derived from our detailed numerical study:

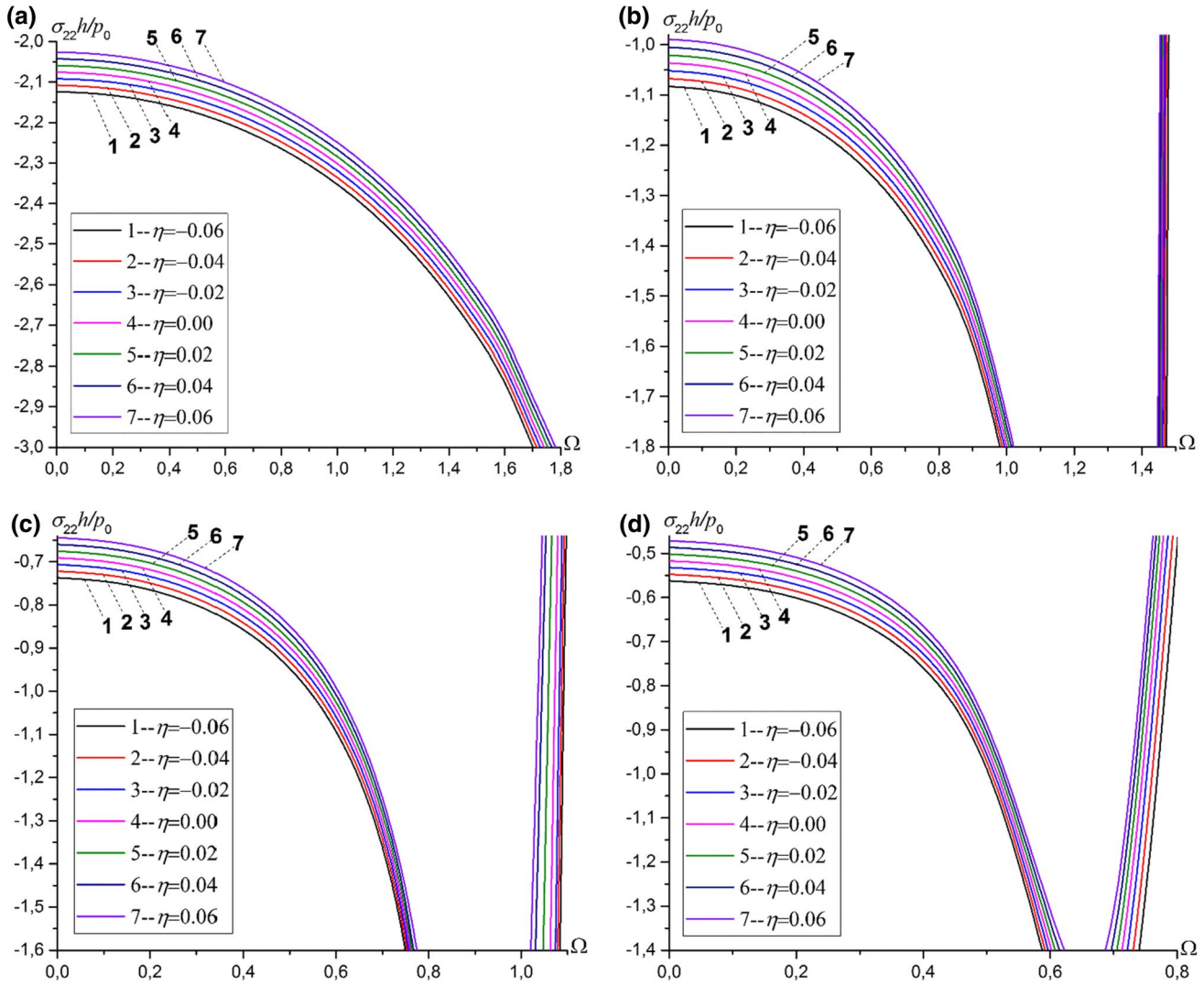

Fig. 6 Variations of $\sigma_{22}h/p_0$ versus Ω for various values of η under **a** $h_* = 0.1$, **b** $h_* = 0.2$, **c** $h_* = 0.3$, and **d** $h_* = 0.4$

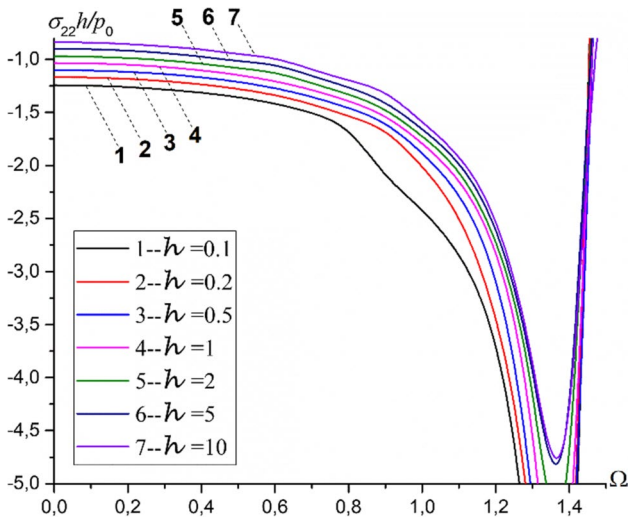

Fig. 7 Variations of $\sigma_{22}h/p_0$ versus Ω for various values of $\hbar$

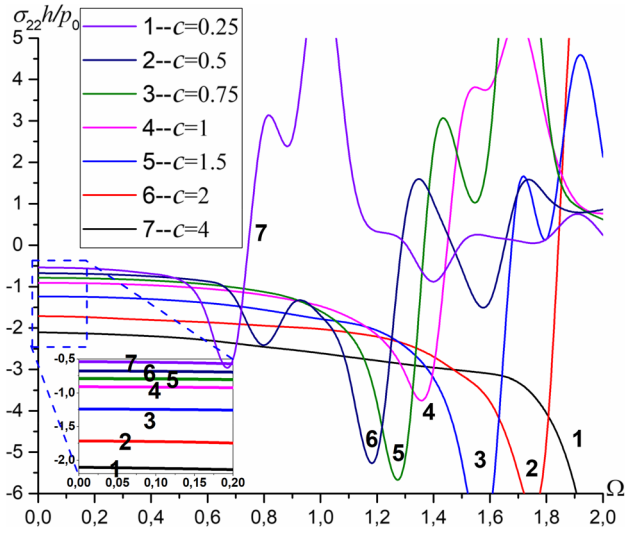

Fig. 8 Variations of $\sigma_{22}h/p_0$ versus Ω for various values of c

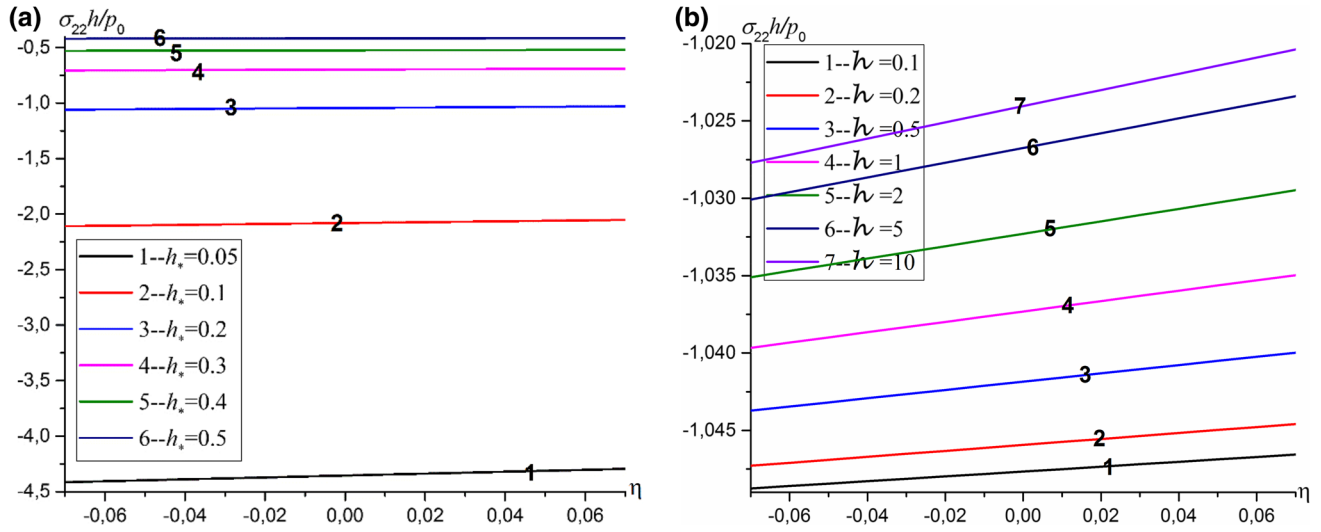

Fig. 9 Variations of $\sigma_{22}h/p_0$ versus η for various values of **a** h_* and **b**η

- an increase in the values of the ratio h_* under fixed initial stress parameter η causes the resonance value $\Omega*$ to decrease;
- an increase in the values of h_* leads to decrease the effect of the parameter η on the dynamic response of $\sigma_{22}h/p_0$;
- an increase in the values of η causes the resonance values of the stress $\sigma_{22}h/p_0$ to prevent;
- and the influence the parameter η has on the frequency response of the plate-strip damps as the values of the ratio h increases;
- the number of local extrema of $\sigma_{22}h/p_0$ with respect to Ω increases with the ratio $\boldsymbol{c}$.

Acknowledgements The author is grateful to the anonymous referees for the time, effort, and extensive comments which improve the quality of the paper. This paper was financially supported by the Research Fund of Kastamonu University under project number KÜBAP-01/2016-4.

References

1. Abad F, Rouzegar J (2017) An exact spectral element method for free vibration analysis of FG plate integrated with piezoelectric layers. Compos Struct 180:696–708
2. Akbarov SD, Guz AN (2000) Mechanics of curved composites. Kluwer Academic Publishers, Dordrecht
3. Abd-alla AN, Alsheikh FA (2009) Reflection and refraction of plane quasi-longitudinal waves at an interface of two piezoelectric media under initial stresses. Arch Appl Mech 79(9):843–857
4. Akbarov SD, Hazar E, Eröz M (2013) Forced vibration of the pre-stressed and imperfectly bonded bi-layered plate strip resting on a rigid foundation. CMC Comput Mat Contin 36(1):23–48
5. Akbarov SD, İlhan N (2013) Time-harmonic Lamb's problem for a system comprising a piezoelectric layer and piezoelectric half-plane. J Sound Vib 332(21):5375–5392
6. Akbarov SD (2015) Dynamics of pre-strained bi-material elastic systems: linearized three-dimensional approach. Springer, New York
7. Akbarov SD, Yahnioglu N (2016) On the total electro-mechanical potential energy and energy release rate at the interface crack tips in an initially stressed sandwich plate-strip with piezoelectric face and elastic core layers. Int J Solids Struct 88:119–130
8. Biezeno CB, Hencky H (1928) On the general theory of elastic stability. Proc R Acad 31:569–592
9. Biot MA (1939) XLIII. Non-linear theory of elasticity and the linearized case for a body under initial stress. Lond Edinb Dublin Philos Mag J Sci 27(183):468–489. https://doi.org/10.1080/14786443908562246
10. Daşdemir A (2017) Effect of imperfect bonding on the dynamic response of a pre-stressed sandwich plate-strip with elastic layers and a piezoelectric core. Acta Mech Solida Sin 30(6):658–667
11. Daşdemir A (2018) A mathematical model for forced vibration of pre-stressed piezoelectric plate-strip resting on rigid foundation. Mat Malay J Ind Appl Math 34(2):419–431
12. D'Ottavio M, Dozio L, Vescovini R, Polit O (2018) The Ritz-Sublaminate generalized unified formulation approach for piezoelectric composite plates. Int J Smart Nano Mater 9(1):34–55
13. Eröz M (2012) The stress field problem for a pre-stressed plate-strip with finite length under the action of arbitrary time-harmonic forces. Appl Math Model 36(11):5283–5292
14. Guo X, Wei P (2014) Effects of initial stress on the reflection and transmission waves at the interface between two piezoelectric half spaces. Int J Solids Struct 51(21–22):3735–3751
15. Green AE, Rivlin RS, Shield RT (1952) General theory of small deformations superposed on large elastic deformations. Proc R Soc A 211:211–292
16. Guz AN (1972) Three-dimensional theory of elastic stability under finite subcritical deformations. Sov Appl Mech 8:1308–1323
17. Guz AN (1999) Fundamentals of the three-dimensional theory of stability of deformable bodies. Springer, New York (translated from Russian by M. Kashtalian)
18. Hutton D (2004) Fundamentals of finite element analysis. McGraw-Hills, New York
19. Ipek C (2015) The dispersion of the flexural waves in a compound hollow cylinder under imperfect contact between layers. Struct Eng Mech 55(2):335–348

20. İlhan N, Koç N (2015) Influence of polled direction on the stress distribution in piezoelectric materials. Struct Eng Mech Int J 54(5):955–971
21. Jiao F, Wei P, Zhou Y, Zhou X (2019) Wave propagation through a piezoelectric semiconductor slab sandwiched by two piezoelectric half-spaces. Eur J Mech-A/Solid 75:70–81
22. Kurt I, Akbarov SD, Sezer S (2016) The influence of the initial stresses on Lamb wave dispersion in pre-stressed PZT/Metal/PZT sandwich plates. Struct Eng Mech 58(2):347–378
23. Neuber H (1943) Die Grundgleichungen der elastischen Stabilität in allgemeinen Koordinaten und ihre Integration. ZAMM-J Appl Math Mech/Z für Angew Math und Mech 23(6):321–330
24. Ogden RW, Sternberg E (1985) Nonlinear elastic deformations. Ellis Horwood/Halsted Press, New York
25. Othmani C, Zhang H, Lü C (2020) Effects of initial stresses on guided wave propagation in multilayered PZT-4/PZT-5A composites: a polynomial expansion approach. Appl Math Model 78:148–168
26. Reddy JN (2003) Mechanics of laminated composite plates and shells: theory and analysis. CRC Press, Florida
27. Sahu SA, Nirwal S, Mondal S (2021) Reflection and transmission of quasi-plane waves at the interface of piezoelectric semiconductors with initial stresses. Appl Math Mech 42(7):951–968
28. Sevdimaliyev YM, Akbarov SD, Guliyev HH, Yahnioglu N (2020) On the natural oscillation of an inhomogeneously pre-stressed multilayered hollow sphere filled with a compressible fluid. Appl Comput Math 19(1):132–146
29. Southwell RV (1914) V. On the general theory of elastic stability. Philosophical transactions of the royal society of London. Ser A Contain Pap Math Phys Charact 213:497–508
30. Yang JS (2005) An introduction to the theory of piezoelectricity. Springer, New York
31. Yeşil Ü (2010) The effect of the initial stretching of the rectangular plate with a cylindrical hole on the stress and displacement distributions around the hole. Turk J Eng Environ Sci 34(1):1–16
32. Tiersten HF (1978) Perturbation theory for linear electroelastic equations for small fields superposed on a bias. J Acoust Soc Am 64(3):832–837
33. Timoshenko S, Godier JN (1951) Theory of elasticity. McGraw Hill, New York
34. Trefftz E (1933) Zur theorie der stabilität des elastischen gleichgewichts. ZAMM-J Appl Math Mech/Z. für Angew Math und Mech 13(2):160–165
35. Uflyand YS (1967) Integral transformations in the theory of elasticity. Nauka, Moscow-Leningrad (**in Russian**)
36. Wen-tao H, Tang-dai X, Wei-yun C (2014) Influence of lateral initial pressure on axisymmetric wave propagation in hollow cylinder based on first power hypo-elastic model. J Cent South Univ 21(2):753–760
37. Zamanov AD, Agasiyev ER (2011) Dispersion of lamb waves in a three-layer plate made from compressible materials with finite initial deformations. Mech Compos Mater 46(6):583–592
38. Zienkiewicz OC, Taylor RL (1989) The finite element method, basic formulation and linear problems. McGraw-Hill, London
39. Zubov IM (1976) Theory of small deformations of prestressed thin-walled shells. J Appl Math Mech 40(1):85–95